Porosity and hole diameter tuning on nanoporous anodic aluminium oxide membranes by one-step anodization

Ugochi K. Chime[1,2], Fabian I. Ezema[2,3], Jose Marques-Hueso[1*]

[1]School of Engineering & Physical Sciences (EPS), Heriot-Watt University, Edinburgh, EH14 4AS, United Kingdom

[2]Department of Physics and Astronomy, University of Nigeria, Nsukka.

[3] Department of Physics, Faculty of Natural and Applied Sciences, Coal City University, Enugu, Nigeria.

*Corresponding author: j.marques@hw.ac.uk

Abstract

Nanoporous Aluminium (III) oxide was fabricated and characterized to determine its suitability as a microfiltration membrane and an antireflection coating. Aluminium (III) oxides were obtained using a one-step anodization process with Phosphoric acid (H_3PO_4) as electrolyte. The effect of the anodization voltage and electrolyte concentration were studied. Semi-ordered nanotubes were observed using a Scanning Electron Microscope. Porosity, pore diameter and interpore distance were obtained and were found to increase with an increase in anodization voltage. While the pore diameter and porosity increased with an increase in electrolyte concentration, the interpore distance was found to remain stable. The porosity was found to vary from 16% to 28% in the investigated range of parameters, while the pore diameter varied from 120 to 178 nm. Reflectance curves showed a wide range of low reflectance in the visible light region, which validates their applicability in the field of anti-reflection coatings.

Key words: Alumina nanotubes; microfiltration membranes; anti-reflection coating;phosphoric acid electrolyte; anodization.

Introduction

Research on non-standard fabrication processes for nanostructured materials has increased in recent years due to their unique properties which are quite different from the bulk form[1]. Nanomaterials have diverse applications including chemical sensing and biosensors[2], oncology[3], DNA translations[4], renewable energy[5] and many more. Well-ordered nanostructures have been fabricated using several techniques such as photolithography[6], X-ray[7], ion-beam[8] and interference lithography[9]. However, these techniques require expensive laboratory equipment.

Porous anodic aluminium oxide (AAO) has attracted a lot of attention due to its self-ordering properties as well as low cost of production[10]. AAO membranes can be used as a template for producing other nanostructures of different sophisticated materials. This can be achieved by depositing these materials into the pores by using several methods such as electrodeposition[11], sol-gel technique[12], atomic layer deposition[13] and chemical vapor deposition[14].

An important application of AAO is in the optical domain. Due to the high band gap of aluminium oxide, the material is transparent in the visible range, and it can be used as antireflection coating. Yang et al. have recently shown that the use of AAO in double-layer anti-reflection coating could increase the efficiency of GaAs solar cells[15]. Due to the porosity, the effective refractive index of AAO can present different values[16], which provides an additional method for controlling its reflectivity. For this reason, it is important to achieve an accurate control on the porosity and hole diameter of the AAO films. Moreover, the graded structures in AAO can be transferred to other materials, conferring them anti-reflective properties[17].Masuda and Fukuda proposed a two-step anodization method, which relies on the use of a long process with oxalic acid and then phosphoric, and it results in well-ordered nanoporous membranes[18]. Since then, several researchers have keyed into two-step processes [19–22], mostly with a hard anodization followed by a mild one. As a result of this, the behaviour of AAO formed from one-step anodization process has been paid little attention due to its non-uniform and disordered pores[21]. However, for industrial applications, the one-step anodization process is a cheaper and less time consuming option.

Porous AAO has also been of significant importance in membrane technology[23–26]. Belwalka et al. showed the effects of applied voltage and electrolyte concentration on the nanopore parameters using sulphuric and oxalic acid electrolytes. The pore sizes ranging from 11nm to 24nm, which are applicable for ultrafiltration applications, were obtained and found to increase with increased voltage and decreased electrolyte concentration[24].Huang et al. proposed that at lower potentials (<17.5V) in sulphuric acid, AAO membranes for nanofiltration applications such as haemodialysis can be fabricated[25]. Microfilters, however, require weaker acids (phosphoric acids) which produce larger pore sizes[27].

Porous AAO is formed through an electrochemical process in which there is an increase in the thickness of the oxide layer on the surface of the aluminium metal[28]. Acidic electrolytes such as oxalic, sulphuric and phosphoric acids are usually used and the oxide growth rate depends on the anodization voltage, electrolyte concentration and electrolyte temperature[21–31]. The best alumina pore uniformity and circularity are obtained at very low temperatures (1°C-5°C)[29].

In this work, nanoporous AAO membranes were fabricated andthe effects of anodization potential and concentration of phosphoric acid on nanoporediameters, interpore distance and porosity were

investigated for the one-step anodization with phosphoric acid. The reflectivity of the obtained membranes was also obtained to determine its suitability as antireflection coating.

Experimental

High purity (99.96%) aluminium foil of 0.05mm thickness cut into dimensions of 12mm by 5mm were first degreased in acetone and then cleaned in a mixed solution of HNO_3:HCl:H_2O in a volumetric ratio of 10:20:70. These cleaned foils were then annealed at 400^0C in Nitrogen atmosphere for 30 minutes. The aluminium foils (anode) were mounted on a copper holder, while a gold coated glass was used as counter electrode. The holder was then placed on the beaker containing the electrolyte in such a way that only the electrodes are immersed with no part of the copper holder touching the solution. The anodization process took place for 10 minutes in a solution with phosphoric acid electrolyte (1-5%). The concentration and cell potential were varied. The electrolyte temperature was maintained at about 3^0C by placing the beaker into an ice bath as shown in Figure 1.

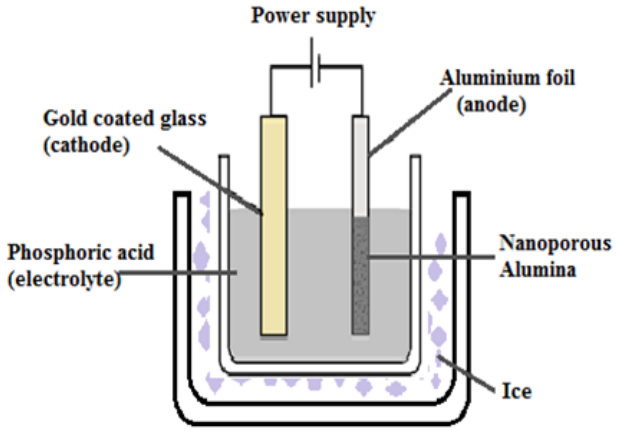

***Figure 1**: Schematic diagram of anodization set-up.*

The morphology of the formed oxide was observed using a Scanning Electron Microscope (SEM). The program Image J was used in measuring the pore diameter, interpore distance, porosity and thickness of the nanotubes. In order to do this, a SEM image of a random location of the sample was opened with the software. The pores were isolated using the "threshold" tool and the area of each hole was measured automatically by the program. The average pore diameter was calculated from the average pore area obtained using the formula for the area of a circle. The porosity has been defined as the percentage of the area that is occupied by holes, and it has been calculated by dividing the total area of the holes measured by the area of the sample section being studied. The interpore distance, defined as the distance from the centres of two adjacent pores, was measured by using the manual tool "length measurement" from the software. An averaged number of 150 holes and 100 interpore distances per sample were

measured to obtain a statistically relevant mean. The thickness of the oxide films have been obtained by SEM imaging of the cross-sectioned samples.

Figure 2 shows the schematic diagram of the used reflectance measurement set up. The light source consists of an Oriel 77501 Fibre Optics Illuminator which transmits the light through a Spectral Product CM110 1/8 metre monochromator which then passes on a selectable range of light wavelength. The detector is used to obtain the relative intensity of reflected light. This is then normalised using polished pure aluminium as a reference and converting to reflectivity using aluminium reflectivity obtained from literature[32].

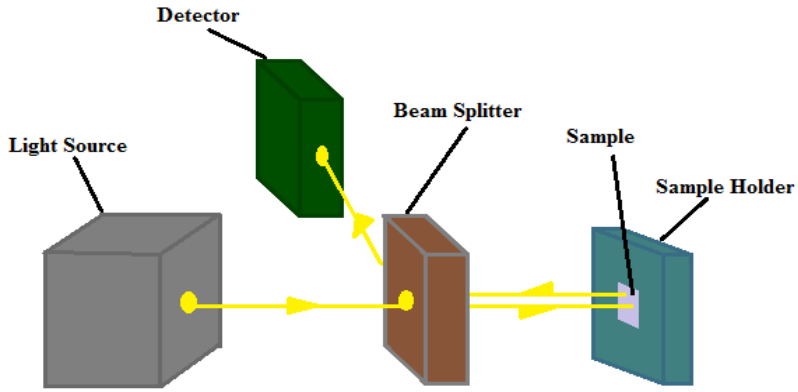

***Figure 2**: Schematic Diagram of local reflectivity measurement set-up.*

Results and discussion

a) Varying Concentration

Figure 3(i) shows the SEM micrographs of the alumina nanopores formed with varied concentrations of phosphoric acid at 150V while Figure 3(ii) shows the effect of the increased concentrations on the pore diameter, interpore distance and the porosity of the formed alumina. It can be observed from the SEM images that in some cases there is a preferential direction for the alignment of the pores. These streaky lines could be due to a preferential direction in the roughness of the substrate, presumable originated by the manufacturing process of the foil. Hence, it should be possible to avoid them by a more intense polishing etch at the pre-treatment. These lines are particularly clear for Figure 3.i.b. In this case the pores are slightly elliptical. For this report, the pores have been approximated to circles. As the concentration of the electrolyte is increased, the averaged pore diameter and the porosity of the nanoporous alumina also increase. However, the increase of the interpore distance is very small, nearly negligible. Although (C) and (D) produced a more ordered arrangement of the nanopores, (A) and (B) produced nanopores with lesser pore diameter which should be targeted to avoid light scattering involved in larger nanotubes. However, unlike in (B), the holes in (A) are not fully formed. Therefore,

a concentration of 1.5 wt% phosphoric acid seems to be a better option for alumina nanopore formation for anti-reflection coating applications.

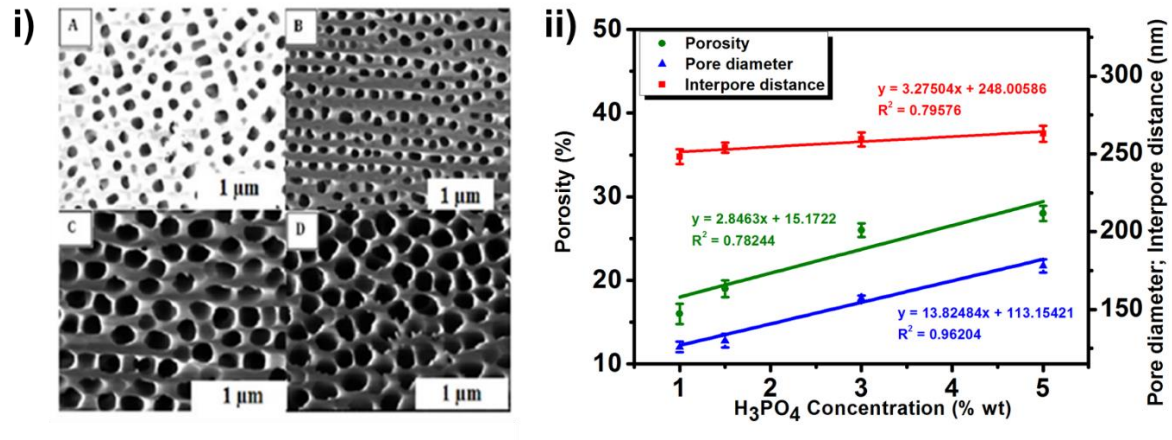

Figure 3*: i) SEM micrographs of nanoporous alumina formed in 10 minutes at 150V with electrolyte H_3PO_4 1wt%(A); 1.5wt%(B); 3wt%(C); 5wt%(D). ii) Interpore distance, pore diameter and porosity vs H_3PO_4 concentration*

b) Varying Voltage

Figure 4(i) shows the SEM images of AAO films obtained at different voltages (130-190 V). It can be seen that the pore distribution varies with the voltage. When fully oxidised, the alumina produced presents deep narrow pores as shown in Figure 4(ii). Figure 4(iii) shows the pore diameter, interpore distance and the porosity with respect to the anodization potential. All the parameters increase with an increase in the voltage. Also, as the pore diameter increases with the interpore distance, it means that at lower voltages, the number of holes formed is greater than those formed at higher voltages. When comparing the reflectivity of these samples with respect to an increase in voltage (Figure 4(iv)), it is seen that in the lower wavelength region, all samples display a high reflectance which decrease sharply and converge at the start of the visible light region. However, towards the long wavelength region, nanopores obtained at low voltages (130 V and 140 V) produced a higher reflectance than samples prepared at higher voltage. On the other hand, the reflectivity curve at 150 V, 170 V and 190 V are almost similar, which denotes a saturating effect. The lower reflectance is due to the increases of hole size, porosity, film thickness and surface roughness. If the porosity increases, then the incoming photons find less flat surfaces to be reflected. Moreover, a higher hole size could result in a higher scattering effect, that would reduce the specular reflectance.

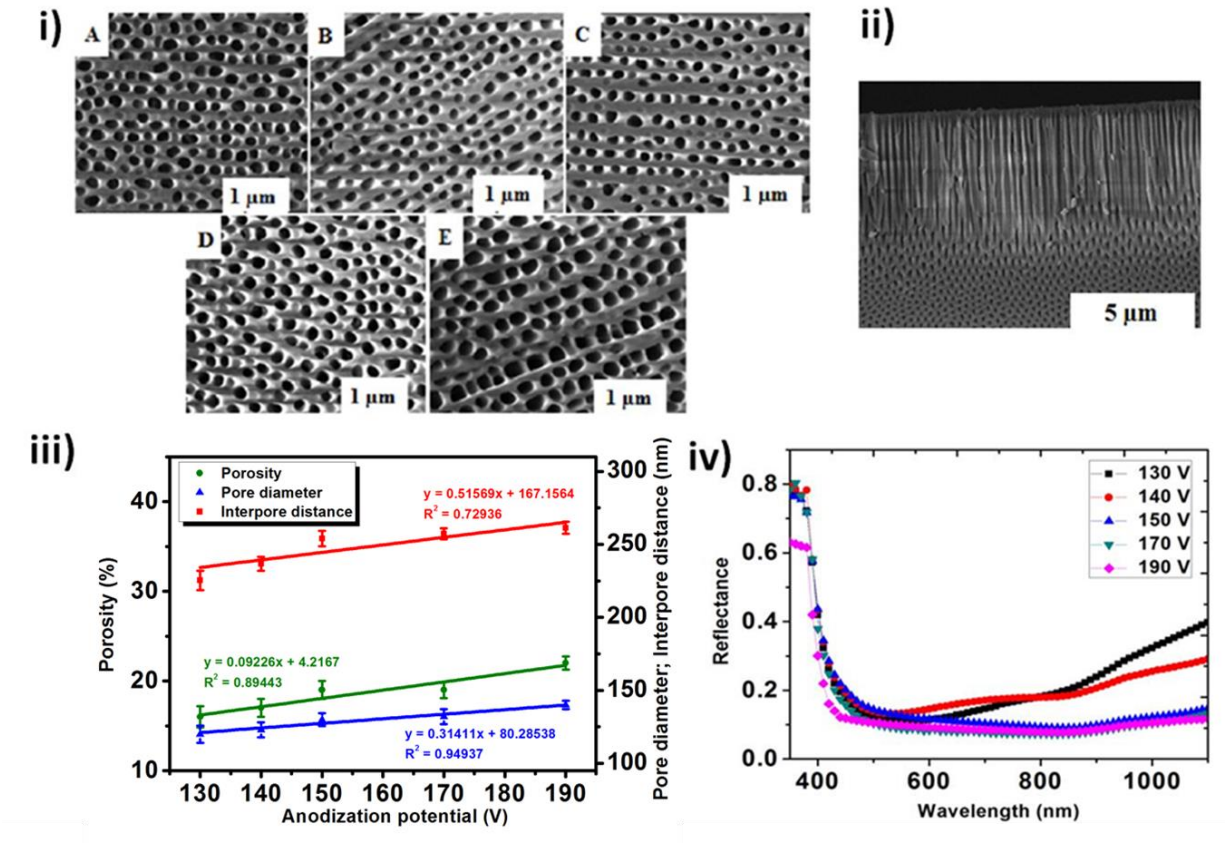

Figure 4: *i) SEM micrographs of nanoporous alumina membranes formed in 10mins in 1.5 wt% H_3PO_4 at 130V (A); 140V (B); 150V (C); 170V (D); 190V (E). ii) Side view of a fully oxidised alumina sample iii) Interpore distance, pore diameter and porosity vs anodization potential. iv) Reflectance of alumina obtained at different anodization potential*

Finally, the thickness of the produced alumina on the side facing the counter-electrode, was obtained using SEM micrographs of the cross section of the samples. Figure 5(i) shows an SEM micrograph of the sample oxidised at 150 V. In this cross-section image it is possible to see that the oxide form a layer on top of the aluminium. This oxide layer is brittle, and it can be damaged during sectioning. Figure 5(ii) shows the cross-section of the sample anodized at 190 V. It is possible to see that the porous oxide layer extends across the whole thickness of the foil sample. The curve in Figure 5(iii) shows the thickness of the formed alumina with respect to the anodization potential. The slow oxide growth rate observed between 130 V and 140 V could be due to a poor charge transport in phosphoric acid at the anodisation potentials. At 150 V, it appears an increase in the charge carrier activities which result in a more rapid oxide growth rate. At 170 V and 190 V both sides of the aluminium samples were oxidised, which means that the front and rear oxide layer had converged. Therefore, in order to obtain a conservative approximated thickness for the front side, the total thickness of the full oxidised sample at these voltages was divided by two. This region of total oxidation is marked in Figure 5(iii) as the Al exhaust layer. Also, though both samples at 170 V and 190 V are fully oxidised, the thickness of the

alumina is found to be different (the initial thickness of the aluminium foil was 50 µm). This is as a result of the different volume expansion ratios of alumina at different anodization potentials which were obtained to be 1.6 and 1.8 respectively. However, it is expected that the film thickness obtained at 170 V and 190 V could be larger if a thicker aluminium foil had been anodised.

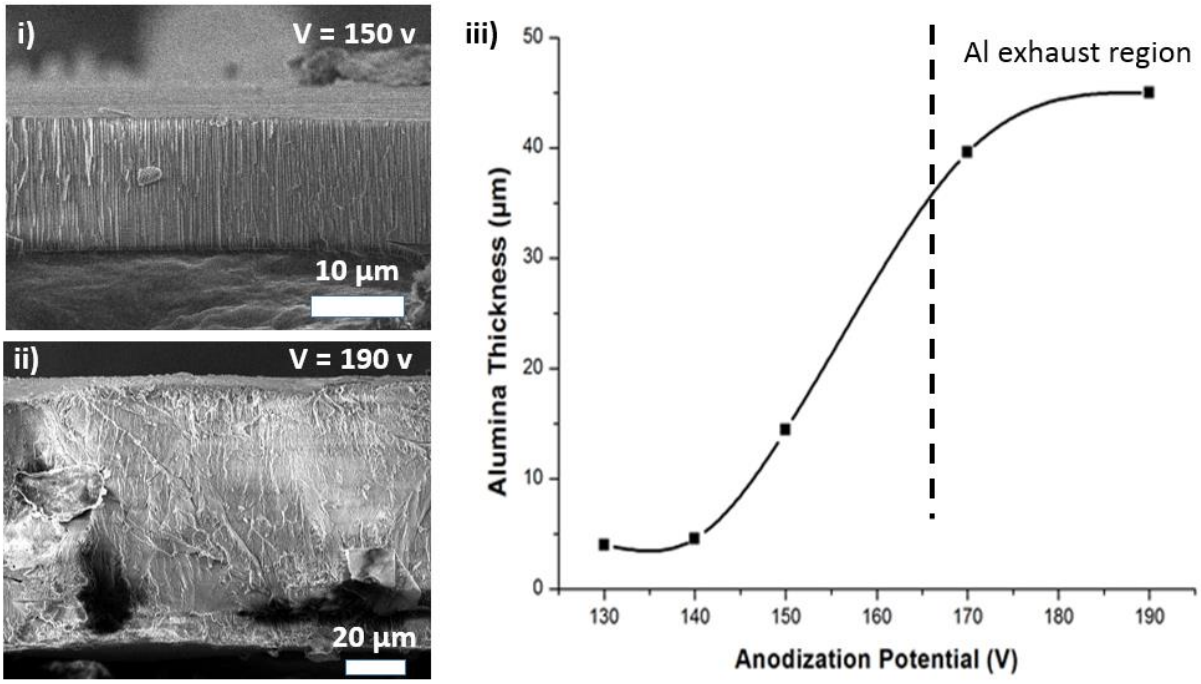

Figure 5*: i) Sample SEM micrograph of cross section of porous alumina (V=150 V). ii) SEM micrograph of cross section (V=190 V) showing a completely oxidized film across the sample. iii) Curve showing an increase in oxide thickness with increased anodization potential.*

Conclusions

Nanoporous arrangements of anodic alumina membranes were obtained in a single step by using phosphoric acid electrolyte. An increase in the electrolyte concentration showed an increase the pore diameter, porosity and only a slight increase in interpore distance. An increase in the cell potential also revealed an increase in the pore diameter, interpore distance, porosity as well as the film thickness. Pore diameters ranging from 120 nm to 178 nm were obtained which enables their use as microfilters. Reflectance curves showed a low reflectance for nanoporous alumina obtained at 150 V, 170 V and 190 V in the visible light region, which indicates that an increase in pore sizes can decrease the reflectance. Hence, with the right chemistry, thin anodic nanopores can be obtained for anti-reflection purposes.

The authors would like to thank Heriot-Watt University for funding.

References

[1] W.J. Stępniowski,, Z. Bojar, Surf. Coat. Technol. 206(2) (2011) 265–72.
[2] A. Santos,, T. Kumeria,, D. Losic, TrAC Trends Anal. Chem. 44 (2013) 25–38.
[3] K.H. Bae,, H.J. Chung,, T.G. Park, Mol. Cells 31(4) (2011) 295–302.
[4] L.Y.T. Chou,, K. Zagorovsky,, W.C.W. Chan, Nat Nano 9(2) (2014) 148–55.
[5] X. Chen,, C. Li,, M. Gratzel,, R. Kostecki,, S.S. Mao, Chem. Soc. Rev. 41(23) (2012) 7909–37.
[6] Masashi Kuwahara and Takashi Nakano and Junji Tominaga and Myung Bok Lee and Nobufumi Atoda Jpn. J. Appl. Phys. 38(9A) (1999) L1079.
[7] F. Tu,, A. Späth,, M. Drost,, F. Vollnhals,, S. Krick Calderon,, R.H. Fink,, H. Marbach, J. Vac. Sci. Technol. B Nanotechnol. Microelectron. Mater. Process. Meas. Phenom. 35(3) (2017)
[8] P. Peinado,, S. Sangiao,, J.M. De Teresa, ACS Nano 9(6) (2015) 6139–46..
[9] Q. Xie,, M.H. Hong,, H.L. Tan,, G.X. Chen,, L.P. Shi,, T.C. Chong, First Int. Symp. Funct. Mater. ISFM2005 449(1) (2008) 261–4.
[10] G.D. Sulka,, W.J. Stępniowski, Electrochimica Acta 54(14) (2009) 3683–91.
[11] K.H. Lee,, Y.P. Huang,, C.C. Wong, Electrochimica Acta 56(5) (2011) 2394–8.
[12] D.N. Kelly,, R.H. Wakabayashi,, A.M. Stacy, ACS Appl. Mater. Interfaces 6(22) (2014) 20122–9.
[13] C. Bae,, H. Shin,, K. Nielsch, MRS Bull. 36(11) (2011) 887–97.
[14] W. Lee,, S.-J. Park, Chem. Rev. 114(15) (2014) 7487–556.
[15] T. Yang,, X. Wang,, W. Liu,, Y. Shi,, F. Yang, Opt. Express 21(15) (2013) 18207–15.
[16] D.W. Thompson,, P.G. Snyder,, L. Castro,, L. Yan,, P. Kaipa,, J.A. Woollam, J. Appl. Phys. 97(11) (2005) 113511.
[17] T. Yanagishita,, T. Kondo,, K. Nishio,, H. Masuda, J. Vac. Sci. Technol. B Microelectron. Nanometer Struct. Process. Meas. Phenom. 26(6) (2008) 1856–9.
[18] H. Masuda,, K. Fukuda, Science 268(5216) (1995) 1466.
[19] M Almasi Kashi and A Ramazani J. Phys. Appl. Phys. 38(14) (2005) 2396.
[20] X.Y. Han,, W.Z. Shen, J. Electroanal. Chem. 655(1) (2011) 56–64.
[21] C.K. Chung,, W.T. Chang,, M.W. Liao,, H.C. Chang,, C.T. Lee, Electrochimica Acta 56(18) (2011) 6489–97.
[22] Z. Liu,, G. Huang,, M. Li,, J. Li,, Y. Chen,, Y. Mei,, R. Liu, Micro- Nano-Eng. MNE 2011 Sel. Contrib. Part I 97 (2012) 147–9.
[23] T. Kyotani,, W. Xu,, Y. Yokoyama,, J. Inahara,, H. Touhara,, A. Tomita, J. Membr. Sci. 196(2) (2002) 231–9.
[24] A. Belwalkar,, E. Grasing,, W.V. Geertruyden,, Z. Huang,, W.Z. Misiolek, J. Membr. Sci. 319(1) (2008) 192–8. [25] Z. Huang,, W. Zhang,, J. Yu,, D. Gao, J. Med. Devices 1(1) (2007) 79–83.
[26] P.P. Mardilovich,, A.N. Govyadinov,, N.I. Mukhurov,, A.M. Rzhevskii,, R. Paterson, J. Membr. Sci. 98(1) (1995) 131–42.
[27] K. Nielsch,, J. Choi,, K. Schwirn,, R.B. Wehrspohn,, U. Gösele, Nano Lett. 2(7) (2002) 677–80.
[28] J. Oh,, C.V. Thompson, Electrochimica Acta 56(11) (2011) 4044–51.
[29] C.K. Chung,, M.W. Liao,, H.C. Chang,, C.T. Lee, 38th Int. Conf. Metall. Coat. Thin Films ICMCTF 2011 520(5) (2011) 1554–8.
[30] G.D. Sulka,, A. Brzózka,, L. Zaraska,, M. Jaskuła, Sens. Sens. Technol. Imagingspectroscopy solidliquid interface 55(14) (2010) 4368–76.
[31] A.P. Li,, F. Müller,, A. Birner,, K. Nielsch,, U. Gösele, J. Appl. Phys. 84(11) (1998) 6023–6.
[32] M. Bass. Handbook of Optics: Volume II - Design, Fabrication, and Testing; Sources and Detectors; Radiometry and Photometry, Third Ed., McGraw Hill Professional, Access Engineering, 2010.